Theoretical Studies of the Structure, Tautomerism, and Vibrational Spectra of 3-Amino-5-nitro-1,2,4-triazole

Dan C. Sorescu,† Carl M. Bennett, and Donald L. Thompson*

Department of Chemistry, Oklahoma State University, Stillwater, Oklahoma 74078

Received: June 3, 1998; In Final Form: October 12, 1998

The structure, tautomerism, and vibrational spectra of the highly explosive 3-amino-5-nitro-1,2,4-triazole (ANTA) molecule were studied by *ab initio* molecular orbital calculations at the Hartree−Fock and second-order (MP2) and fourth-order (MP4) Möller−Plesset levels and by density functional theory (DFT) both in gas phase and in solution. It was found that in the gas phase the most stable tautomer is 2*H*-ANTA (3-amino-5-nitro-1,2,4-2*H*-triazole) at the HF level, while at MP2, MP4, and DFT levels the most stable tautomer is 1*H*-ANTA (3-amino-5-nitro-1,2,4-1*H*-triazole). For the 2*H*-ANTA tautomer, the calculated MP2 and DFT structures agree well with the experimental X-ray structures, but with the twisting of the nitro and amino groups much larger than in the solid state. The predicted IR spectra are given for all tautomers. The calculated fundamental vibrational frequencies at the DFT level generally compare well with the MP2 results. In the case of 2*H*-ANTA, the C−NO_2, C−NH_2, and N−H bond dissociation energies were estimated to be 67.1, 112.8, and 97.2 kcal/mol, respectively. On the basis of the structural and spectroscopic results calculated at the MP2 level, a classical force field for gas-phase 2*H*-ANTA was developed. The effects of environment polarity on the conformations and energetics of 1*H*-ANTA and 2*H*-ANTA tautomers were studied by performing calculations at the DFT level within the Onsager continuum solvation model. The results obtained for the dielectric constants $\epsilon = 4.8$, 18.5, and 78.4 suggest that in a polar solvent the most stable tautomer is 2*H*-ANTA, in agreement with the experimental studies.

1. Introduction

Experimental studies performed in the past decade have identified the crystalline form of 3-amino-5-nitro-1,2,4-2*H*-triazole (2*H*-ANTA) (see Figure 1) as an insensitive highly explosive material, with characteristics that make it well-suited for a variety of defense and civilian applications.[1,2] The sensitivity of an explosive depends on properties such as shear strength and molecular orientations of the crystalline material[3] as well as the early steps of chemical reaction.[4] Ultimately, understanding the thermal decomposition mechanism of an energetic material is important if we are to explain its low sensitivity. And, of course, it is important to understand the underlying fundamental properties of materials that determine their sensitivity.

The structures of crystalline ANTA have been resolved by X-ray crystallography.[5,6] Two polymorphic phases, α and β, have been identified. The α phase is obtained by growth from an ethanol and chloroform mixture. It has a monoclinic crystallographic structure with $C2/c$ symmetry and $Z = 8$ molecules per unit cell. The molecular arrangement is that of twisted ribbons.[5] The β-ANTA is obtained by recrystallization from 2-butanone.[6] This phase has $P2_1/n$ symmetry with $Z = 4$ molecules per unit cell and is characterized by extended planar molecular sheets.

A theoretical study of gas-phase ANTA has been reported by De Paz and Ciller,[7] in which the tautomers of ANTA were treated by using semiempirical AM1 and PM3 theory and at the ab initio RHF/6-31G(d)//RHF/6-31G level.[8] They found that 2*H*-ANTA is the most stable tautomer and that 1*H*- and 4*H*-ANTA (see Figure 2) are less stable, by 2 and 7.4 kcal/mol, respectively, at the RHF/6-31G(d)//RHF/6-31G level of theory. The molecular structural parameters determined in that study indicate that the ring and the substituents are in the same molecular plane; i.e., there is no twist of the NO_2 group or pyramidalization of the NH_2 substituent. These results[7] are in disagreement with the experimental X-ray structure of α-ANTA,[5] in which the nitro group is twisted out of the plane by 10.5° and the amino group by 5.4°. Further insight in the relative stability of the tautomers was obtained by calculation of their dipole moments, which were found to vary in the order 2*H*-ANTA > 4*H*-ANTA ≫ 1*H*-ANTA. These results support the experimental findings, which indicate that 2*H*-ANTA is the most stable tautomer in a polar solvent.[5]

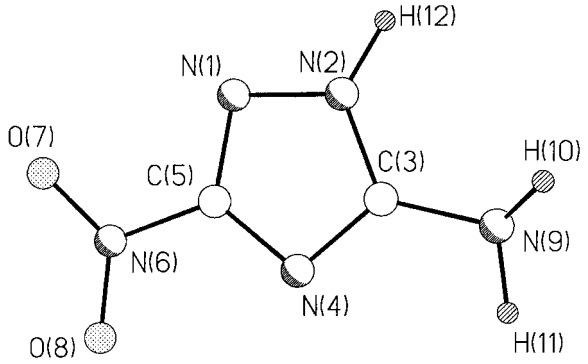

Figure 1. Atom designation and numbering for the 2*H*-ANTA molecule.

In an attempt to better characterize the geometric and spectroscopic parameters of ANTA in the gas phase, we report

† Current mailing address: Department of Chemistry, University of Pittsburgh, Pittsburgh, PA 15260.

10.1021/jp9824712 CCC: $15.00
Published on Web 11/20/1998

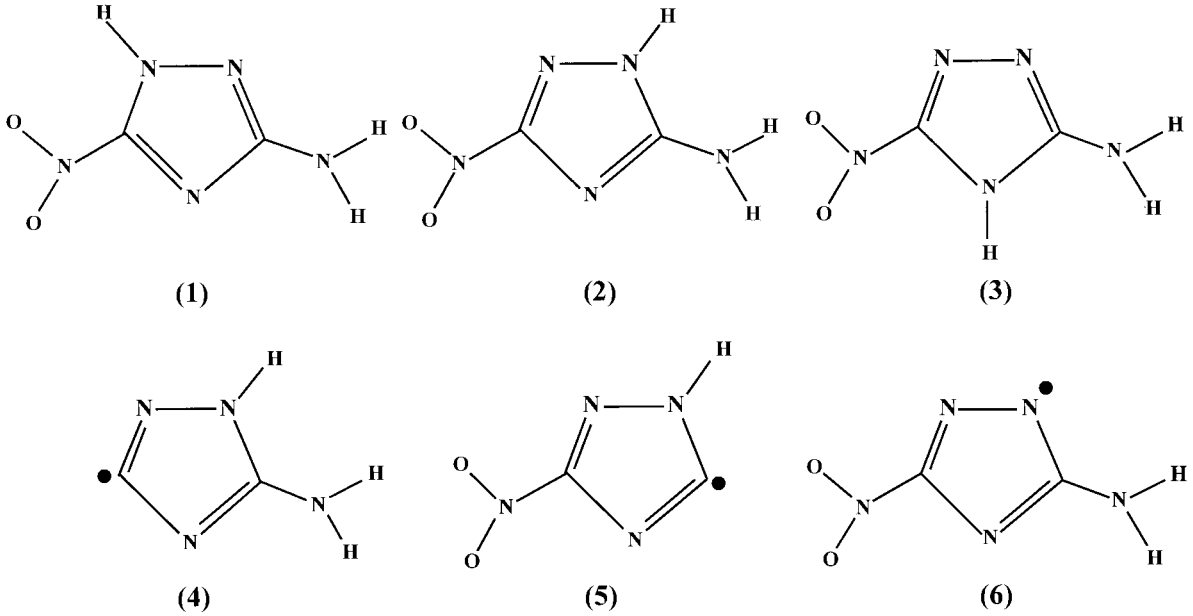

Figure 2. ANTA tautomers and radicals.

here the results of ab initio calculations at the Hartree−Fock (HF) and second-order Möller−Plesset (MP2)[9] levels, using various basis sets. We have previously used density functional theory (DFT) in the Kohn−Sham formulation[10] as an alternative to the computationally demanding (for molecules of the size of interest here) MP2 method. The DFT method offers a less expensive but still accurate computational alternative to ab initio methods that include electron correlation in post-HF treatments. Numerous studies in the past couple of years have shown that nonlocal DFT techniques can be superior to the Hartree−Fock theory for calculating molecular force fields and are in some cases closer to or even better than the MP2 methods.[11−14]

In addition to the energetic and geometrical parameters, we also report ab initio values for the fundamental vibrational frequencies. These were calculated for the ANTA tautomers using analytical second derivatives at the optimized geometries. Ideally, the interpretation and the accuracy of the theoretical frequencies should be done by making comparisons to gas-phase experimental results. However, measured spectra for ANTA are unavailable. We hope that the results reported here will stimulate measurements of them.

Some insight into the decomposition mechanisms can be obtained by studying homolytic bond cleavage of ANTA. For this purpose we calculated the energies and the structures of the radicals that result from elimination of the nitro and amino groups and of atomic hydrogen and estimated the corresponding $C-NO_2$, $C-NH_2$, and N−H bond dissociation energies.

The approach followed in this study is similar to that used to investigate the geometric and spectroscopic parameters of 5-nitro-2,4-dihydro-3*H*-1,2,4-triazol-3-one (NTO).[15] That study showed that Becke's three-parameter hybrid method,[16] in combination with the Lee, Yang, and Parr correlation functional (B3LYP),[17] provides results for the NTO molecule comparable to those computed at the MP2 level. The calculated values of the geometric parameters at the MP2 and B3LYP levels are in fairly good agreement with each other and with the experimental geometry of the β-NTO crystal (except for the N−H bond lengths for which no accurate experimental values are available). Moreover, the calculated MP2 and B3LYP vibrational frequencies agree very well with the experimental values determined from IR spectra of NTO isolated in an argon matrix at 21 K.[15] These spectra consist of well-defined, narrow infrared bands, indicative of minimal intermolecular interactions. We also observed that the environment in the NTO crystal has a strong influence on the spectral features of the NTO molecule. For example, the spectra of thin films of pure NTO display significant differences from those of NTO isolated in an argon matrix, with extensive broadening and large frequency shifts, due to strong intermolecular interactions in the polycrystalline phase.

We also performed ab initio calculations with inclusion of the solvent effects to qualitatively determine the influence of a solvent environment on the energetic and structural parameters of ANTA. These were done by using the self-consistent reaction field model,[18] with a uniform dielectric constant.

Insight in the dynamical aspects of the thermal decomposition of ANTA could be obtained by using molecular dynamics calculations if an accurate potential energy surface (PES) that describes the main geometric, spectroscopic, and thermochemical parameters of the reactant, products, and transition states were formulated. We have previously developed and used such PESs in molecular dynamics and Monte Carlo simulations of a number of cyclic nitro and diaza compounds, such as hexahydro-1,3,5-trinitro-1,3,5-triazine (RDX)[19,20] and 2,3-diazabicyclo-[2.2.1]hept-2-ene.[21,22] In the present paper, we undertake the first step in the development of a reliable PES for ANTA by constructing a force field for the 2*H*-ANTA molecule in the gas phase. This force field is based on the geometries and the scaled fundamental frequencies determined predicted by ab initio calculations at the MP2/6-311+G(d,p) level.

2. Computational Procedure

Standard ab initio molecular orbital calculations were carried out using the Gaussian-94 programs.[23] The geometries of 1*H*-, 2*H*-, and 4*H*-ANTA tautomers and the radicals corresponding to homolytic bond cleavages in 2*H*-ANTA have been optimized using the 6-31G(d,p) (split-valence plus d-type and p-type polarization functions), 6-311G(d,p) (triple-ζ-valence plus d-type and p-type polarization functions), and 6-311+G(d,p) (triple-ζ-valence functions plus dp-polarization and diffuse functions) basis sets,[8,24] under the C_1 symmetry. The optimizations were initially done at the (U)HF level and then refined at the (U)-

MP2 level. All geometry optimizations met the default convergence criteria given by Gaussian-94.[23] The frozen-core approximation was employed in the MP2 calculations.

The DFT calculations were done using BLYP and B3LYP exhange-correlation functionals. The BLYP uses the gradient-corrected exchange functional of Becke[25] and the gradient-corrected correlation energy functional of Lee, Yang, and Parr[17] (BLYP), while the B3LYP uses the exchange functional described by the fitted three-parameter hybrid of Becke[16] and the correlation functional of Lee, Yang, and Parr (B3LYP). The geometry optimizations were performed with 6-31G** and 6-311+G(d,p) bases.

The nature of all stationary points determined at the HF, MP2, and DFT levels were determined by calculating the vibrational frequencies. The calculated frequencies and the corresponding intensities were used to predict the IR spectra. The values of harmonic vibrational frequencies determined at various levels have been uniformly scaled by 0.8929 at HF/6-31G(d,p), 0.8970 at HF/6-311+G(d,p), 0.9370 at MP2/6-31G(d,p), 0.9496 at MP2/6-311G(d,p), 0.95 at MP2/6-311+G(d,p), 0.9613 at both B3LYP/6-31G(d,p) and B3LYP/6-311+G(d,p), and 0.9945 at BLYP/6-31G(d,p) and BLYP/6-311+G(d,p) levels,[14,18,26] to correct for the overestimation of vibrational frequencies.

We also performed calculations using the Onsager self-consistent reaction field (SCRF) model,[27,28] as implemented in the Gaussian-94 program, to determine the qualitative effects produced by a polar environment on equilibrium conformations as well as on the energies and vibrational frequencies of the 1*H*- and 2*H*-ANTA molecules. In this model, the solute molecule is placed in a spherical cavity surrounded by a continuum with constant dielectric properties. The molecular dipole induces a dipole in the dielectric medium and the electric field applied to the solute by the solvent dipole in turn interacts with the molecular dipole, reducing the energy of the solute. Because only electrostatic effects are included in the Onsager model, and other effects such as the cavity work, dispersion, and exchange repulsion are neglected, the model is most applicable to polar molecules in polar solvents. We have investigated solvents with dielectric constants of 4.806 D (chloroform), 18.5 D (2-butanone), and 78.4 D (water). In each case the radius of the spherical cavity occupied by the solute was estimated based on molecular volume calculations as implemented in the Gaussian-94 program.[23]

3. Results and Discussion

Geometries. The tautomers studied in the present work are 1*H*-ANTA, 2*H*-ANTA, and 4*H*-ANTA; they are illustrated in Figure 2. The atom designation and numbering used in the tables and in the present discussion are shown in Figure 1. The hydrogen atom H_{12} is bound to atoms N_1, N_2, or N_4 in 1*H*-, 2*H*-, and 4*H*-ANTA, respectively. The values of the geometrical parameters of these tautomers predicted at the HF, MP2, and DFT levels are given in Table 1 and supplementary Tables 1S−3S. The values given in parentheses in Table 1 are the absolute percent differences between the values computed at the various levels of theory and those computed at the MP2/6-311+G(d,p) level.

First we will focus on the description of the geometry of the 2*H*-ANTA molecule, for which experimental X-ray data are available. As can be seen from Table 1, the predicted structure of 2*H*-ANTA is nonplanar at the HF/6-31G(d,p) level. This is in disagreement with the planar structure reported by De Paz and Ciller[7] based on ab initio calculations at the HF/3-21G and HF/6-31G levels. In the HF/6-31G(d,p) structure (see Table 1), the ring and the NO_2 and NH_2 groups are not in the same plane. The NO_2 group is twisted and the NH_2 group is pyramidal, in agreement with the experimental structure of α-ANTA.[5] These geometrical features are also predicted when much larger basis sets, such as HF/6-311+G(d,p), are used (see Table 1). A possible explanation for the absence of pyramidalization in the structure predicted by HF/6-31G is the lack of polarization functions in the basis set. Indeed, it has been shown[29] that these functions are necessary to correctly describe the pyramidalization of an amino group. In the solid phase, the crystal packing effects and hydrogen bonding interactions might result in different orientations of the amino and nitro groups. For example, we can see by comparing the dihedral angles of the experimental α-ANTA and *β*-ANTA structures in Table 1 that in the case of the *β* structure, the NO_2 group is not twisted and that there is a much smaller pyramidalization of the amino group; the angle $N_2-C_3-N_9-H_{10}$ changes from −18.6° to 8.1° and the angle $N_4-C_3-N_9-H_{11}$ from 8.8° to −0.1°.

Inclusion of electron correlation in post-HF calculations produces several effects. There are some significant differences from the HF results at the MP2 level in some bond lengths; for example, the absolute percent differences between the HF/6-311+G(d,p) and the MP2/6-311+G(d,p) values for the double bonds C_5N_1 and C_3N_4 are 4.1% and 2.1%, respectively, and 3.9% and 4.0% for the two N−O bonds. There are no significant differences in the values of the bond angles computed at the HF to MP2 levels, except for the $C_3-N_9-H_{10}$ and $C_3-N_9-H_{11}$ angles, for which the differences are 2.1% and 2.4%, respectively.

We also investigated the dependence of the geometrical parameters on the basis set. At the MP2 level the bond lengths are practically independent of the basis set employed, with variations of less than 1.0%. Also, the bond angles and the majority of ring dihedral angles are similarly independent of the basis set. However, there is a pronounced variation of the twist of the nitro group relative to the ring plane in the case of optimization with the diffuse basis set MP2/6-311+G(d,p).

The gas-phase structure of ANTA determined at the MP2 level and the experimental X-ray data (see Table 1) are in good agreement. For the heavy atoms, the largest differences are 0.041 Å for bond lengths and 2.4° for bond angles. For the angles in which hydrogen atoms are involved, the largest difference is 4.57°, for the $C_3-N_9-H_{10}$ angle. It is difficult to compare the calculated N−H bond lengths with the experimental values for the α- or *β*-ANTA structures since the coordinates of hydrogen atoms are not precisely determined by X-ray diffraction. Indeed, it is known[30] that X-ray diffraction measurements indicate a shift of electron density into the bond, while other methods, such as neutron diffraction or microwave spectroscopy, indicate the nuclear positions.

The geometrical parameters in the case of B3LYP and BLYP calculations are generally very close to the MP2 results and represent, as expected, definite improvement over the HF results. The maximum deviations from MP2 values for the bond lengths are 1.4% at B3LYP/6-311+G(d,p) level and 1.8% at BLYP/6-311+G(d,p) level, while for the bond angles, the corresponding maximum differences are 2.7% and 2.5%, respectively. Generally, there are small differences in the results calculated using the 6-31G(d,p) and 6-311+G(d,p) basis sets. Moreover, the predicted dihedral angles involving the nitro group at both the B3LYP and BLYP levels are in better accord with the MP2/6-31G(d,p) and MP2/6-311G(d,p) results, i.e., no large twists of the NO_2 group. Similar conclusions can be drawn from the analyses of the geometries of the other two tautomers, 1*H*-

TABLE 1: Selected Geometrical Parameters for 1*H*-, 2*H*-, and 3*H*-ANTA Molecules[a]

parameter	HF 6-31G(d,p)	HF 6-311+G(d,p)	MP2 6-31G(d,p)	MP2 6-311G(d,p)	MP2 6-311+G(d,p)	B3LYP 6-31G(d,p)	B3LYP 6-311+G(d,p)	BLYP 6-31G(d,p)	BLYP 6-311+G(d,p)	Exp. ref 5	Exp. ref 6
					1H-ANTA						
$r(N_1-N_2)$	1.3456 (0.0)	1.3448 (0.1)	1.3509 (0.4)	1.3463 (0.0)	1.3460	1.3539 (0.6)	1.3525 (0.5)	1.3688 (1.7)	1.3665 (1.5)		
$r(N_2-C_3)$	1.3039 (3.4)	1.3007 (3.6)	1.3520 (0.2)	1.3480 (0.1)	1.3499	1.3435 (0.5)	1.3389 (0.8)	1.3637 (1.0)	1.3589 (0.7)		
$r(C_3-N_4)$	1.3568 (0.3)	1.3578 (0.2)	1.3616 (0.1)	1.3606 (0.0)	1.3602	1.3644 (0.3)	1.3631 (0.2)	1.3755 (1.1)	1.3730 (0.9)		
$r(N_4-C_5)$	1.2864 (2.8)	1.2837 (3.0)	1.3249 (0.1)	1.3214 (0.1)	1.3233	1.3157 (0.6)	1.3113 (0.9)	1.3314 (0.6)	1.3267 (0.3)		
$r(C_5-N_1)$	1.3130 (2.6)	1.3126 (2.6)	1.3475 (0.0)	1.3469 (0.1)	1.3480	1.3416 (0.5)	1.3398 (0.6)	1.3578 (0.7)	1.3561 (0.6)		
$r(C_5-N_6)$	1.4454 (0.1)	1.4529 (0.6)	1.4373 (0.5)	1.4438 (0.0)	1.4439	1.4450 (0.1)	1.4524 (0.6)	1.4547 (0.7)	1.4616 (1.2)		
$r(N_6-O_7)$	1.1979 (3.2)	1.1919 (3.7)	1.2489 (0.9)	1.2358 (0.2)	1.2380	1.2380 (0.0)	1.2322 (0.5)	1.2609 (1.8)	1.2555 (1.4)		
$r(N_6-O_8)$	1.1811 (3.8)	1.1740 (4.4)	1.2397 (0.9)	1.2261 (0.2)	1.2282	1.2217 (0.5)	1.2146 (1.1)	1.2428 (1.2)	1.2362 (0.7)		
$r(C_3-N_9)$	1.3639 (1.1)	1.3660 (0.9)	1.3785 (0.0)	1.3795 (0.0)	1.3791	1.3697 (0.7)	1.3679 (0.8)	1.3796 (0.0)	1.3765 (0.2)		
$r(N_9-H_{10})$	.9944 (1.6)	0.9950 (1.6)	1.0088 (0.2)	1.0102 (0.1)	1.0110	1.0094 (0.2)	1.0083 (0.3)	1.0178 (0.7)	1.0160 (0.5)		
$r(N_9-H_{11})$	.9943 (1.6)	0.9949 (1.6)	1.0085 (0.2)	1.0099 (0.1)	1.0107	1.0092 (0.2)	1.0082 (0.3)	1.0176 (0.7)	1.0158 (0.5)		
$r(N_1-H_{12})$	0.9934 (1.9)	0.9937 (1.8)	1.0094 (0.3)	1.0109 (0.1)	1.0123	1.0099 (0.2)	1.0098 (0.3)	1.0179 (0.6)	1.0177 (0.5)		
$\tau(N_1-C_5-N_6-O_7)$	0.62	0.45	0.71	0.66	0.67	0.33	0.29	0.29	0.26		
$\tau(N_4-C_5-N_6-O_8)$	0.59	0.29	0.30	0.43	0.06	0.30	0.04	0.17	0.00		
$\tau(N_2-C_3-N_9-H_{10})$	20.49	21.34	25.68	25.83	25.76	21.76	20.56	22.91	20.89		
$\tau(N_4-C_3-N_9-H_{11})$	−24.49	−25.31	−28.49	−29.02	−28.00	−23.59	−22.19	−24.33	−22.01		
					2*H*-ANTA						
$r(N_1-N_2)$	1.3466 (0.6)	1.3456 (0.6)	1.3581 (0.3)	1.3538 (0.0)	1.3541	1.3615 (0.6)	1.3594 (0.4)	1.3787 (1.8)	1.3763 (1.6)	1.3687	1.3673
$r(N_2-C_3)$	1.3392 (1.5)	1.3390 (1.5)	1.3589 (0.0)	1.3588 (0.0)	1.3592	1.3633 (0.3)	1.3625 (0.2)	1.3783 (1.4)	1.3777 (1.4)	1.3499	1.3506
$r(C_3-N_4)$	1.3014 (2.0)	1.2999 (2.1)	1.3298 (0.1)	1.3270 (0.1)	1.3285	1.3237 (0.4)	1.3204 (0.6)	1.3373 (0.7)	1.3335 (0.4)	1.3336	1.3406
$r(N_4-C_5)$	1.3419 (0.7)	1.3417 (0.8)	1.3529 (0.1)	1.3514 (0.0)	1.3520	1.3545 (0.2)	1.3521 (0.0)	1.3673 (1.1)	1.3641 (0.9)	1.3439	1.3412
$r(C_5-N_1)$	1.2801 (3.8)	1.2766 (4.1)	1.3345 (0.3)	1.3303 (0.0)	1.3308	1.3171 (1.0)	1.3116 (1.4)	1.3355 (0.4)	1.3293 (0.1)	1.3085	1.3012
$r(C_5-N_6)$	1.4523 (0.3)	1.4593 (0.1)	1.4523 (0.3)	1.4589 (0.1)	1.4573	1.4619 (0.3)	1.4689 (0.8)	1.4756 (1.3)	1.4829 (1.8)	1.4467	1.4452
$r(N_6-O_7)$	1.1900 (3.3)	1.1835 (3.9)	1.2415 (0.9)	1.2285 (0.2)	1.2310	1.2275 (0.3)	1.2210 (0.8)	1.2479 (1.4)	1.2418 (0.9)	1.2256	1.2224
$r(N_6-O_8)$	1.1884 (3.5)	1.1822 (4.0)	1.2414 (0.9)	1.2285 (0.2)	1.2310	1.2265 (0.4)	1.2202 (0.9)	1.2468 (1.3)	1.2410 (0.8)	1.2205	1.2251
$r(C_3-N_9)$	1.3599 (1.6)	1.3616 (1.5)	1.3830 (0.0)	1.3830 (0.0)	1.3825	1.3721 (0.7)	1.3693 (1.0)	1.3843 (0.1)	1.3803 (0.2)	1.3408	1.3330
$r(N_9-H_{10})$	0.9950 (1.7)	0.9954 (1.7)	1.0106 (0.2)	1.0117 (0.1)	1.0123	1.0110 (0.1)	1.0093 (0.3)	1.0199 (0.7)	1.0173 (0.5)	0.8819	0.8559
$r(N_9-H_{11})$	.9957 (1.7)	0.9961 (1.6)	1.0109 (0.2)	1.0121 (0.1)	1.0127	1.0115 (0.1)	1.0101 (0.3)	1.0200 (0.7)	1.0180 (0.5)	0.8743	0.8330
$r(N_2-H_{12})$	.9929 (1.8)	0.9930 (1.8)	1.0087 (0.3)	1.0101 (0.1)	1.0112	1.0095 (0.2)	1.0091 (0.2)	1.0179 (0.7)	1.0172 (0.6)	0.8437	0.8496
$\theta(C_3-N_9-H_{10})$	117.23 (2.4)	116.83 (2.1)	113.84 (0.5)	116.66 (1.9)	117.49 (2.7)	116.08 (1.4)	117.29 (2.5)	117.29 (2.5)	119.00	120.09	
$\theta(C_3-N_9-H_{11})$	113.45 (2.4)	113.45 (2.3)	110.18 (0.6)	110.09 (0.7)	110.84	112.33 (1.3)	113.46 (2.4)	111.69 (0.8)	113.22 (2.1)	114.23	117.25
$\tau(N_1-C_5-N_6-O_7)$	−2.58	−7.31	−3.58	−3.69	−22.25	−1.32	−2.29	−1.47	−2.49	−11.05	−0.29
$\tau(N_4-C_5-N_6-O_8)$	−3.00	−7.59	−4.53	−4.28	−22.48	−1.79	−2.63	−1.97	−2.80	−9.94	0.38
$\tau(N_2-C_3-N_9-H_{10})$	35.27	35.46	52.44	50.36	50.74	39.10	35.81	40.81	36.52	−18.62	8.07
$\tau(N_4-C_3-N_9-H_{11})$	−10.90	−11.98	−7.19	−9.31	−7.40	−11.72	−11.68	−13.01	−12.61	8.82	−0.13
					3*H*-ANTA						
$r(N_1-N_2)$	1.3562 (1.5)	1.3571 (1.5)	1.3819 (0.3)	1.3774 (0.0)	1.3771	1.3690 (0.6)	1.3666 (0.8)	1.3869 (0.7)	1.3828 (0.4)		
$r(N_2-C_3)$	1.2971 (2.2)	1.2938 (2.5)	1.3293 (0.2)	1.3248 (0.2)	1.3268	1.3313 (0.3)	1.3269 (0.0)	1.3487 (1.7)	1.3444 (1.3)		
$r(C_3-N_4)$	1.3473 (1.4)	1.3487 (1.3)	1.3657 (0.1)	1.3658 (0.1)	1.3666	1.3614 (0.4)	1.3612 (0.4)	1.3733 (0.5)	1.3730 (0.5)		
$r(N_4-C_5)$	1.3599 (0.0)	1.3599 (0.0)	1.3594 (0.1)	1.3591 (0.1)	1.3605	1.3735 (1.0)	1.3734 (1.0)	1.3865 (1.9)	1.3869 (1.9)		
$r(C_5-N_1)$	1.2675 (3.6)	1.2632 (3.9)	1.3183 (0.3)	1.3135 (0.1)	1.3149	1.3050 (0.8)	1.2992 (1.2)	1.3228 (0.6)	1.3170 (0.2)		
$r(C_5-N_6)$	1.4317 (1.0)	1.4392 (0.5)	1.4395 (0.5)	1.4466 (0.0)	1.4467	1.4338 (0.9)	1.4387 (0.6)	1.4445 (0.2)	1.4488 (0.1)		
$r(N_6-O_7)$	1.1824 (3.5)	1.1748 (4.1)	1.2370 (0.9)	1.2235 (0.2)	1.2254	1.2229 (0.2)	1.2159 (0.8)	1.2438 (1.5)	1.2373 (1.0)		
$r(N_6-O_8)$	1.2010 (3.0)	1.1955 (3.4)	1.2480 (0.8)	1.2352 (0.2)	1.2379	1.2418 (0.3)	1.2369 (0.1)	1.2648 (2.2)	1.2609 (1.9)		
$r(C_3-N_9)$	1.3650 (1.4)	1.3663 (1.3)	1.3848 (0.1)	1.3852 (0.1)	1.3839	1.3701 (1.0)	1.3670 (1.2)	1.3804 (0.3)	1.3761 (0.6)		
$r(N_9-H_{10})$	0.9969 (1.7)	0.9971 (1.7)	1.0120 (0.2)	1.0133 (0.1)	1.0139	1.0122 (0.2)	1.0108 (0.3)	1.0207 (0.7)	1.0187 (0.5)		
$r(N_9-H_{11})$	0.9963 (1.7)	0.9966 (1.6)	1.0117 (0.2)	1.0129 (0.0)	1.0133	1.0113 (0.2)	1.0095 (0.4)	1.0198 (0.6)	1.0173 (0.4)		
$r(N_4-H_{12})$	0.9940 (1.8)	0.9941 (1.8)	1.0091 (0.3)	1.0105 (0.1)	1.0120	1.0099 (0.2)	1.0098 (0.2)	1.0181 (0.6)	1.0179 (0.6)		
$\tau(N_1-C_5-N_6-O_7)$	0.22	0.23	0.90	0.54	0.79	0.42	0.62	0.45	0.66		
$\tau(N_4-C_5-N_6-O_8)$	−0.38	−0.50	−0.64	−0.55	−1.49	−0.38	−0.41	−0.40	−0.42		
$\tau(N_2-C_3-N_9-H_{10})$	7.20	8.14	2.73	3.14	3.59	10.06	10.16	11.64	11.23		
$\tau(N_4-C_3-N_9-H_{11})$	−43.80	−43.74	−59.28	−58.93	−57.08	−41.35	−37.84	−41.52	−36.96		

[a] The values in parentheses correspond to percentage differences relative to MP2/6-311+G(d,p) results.

TABLE 2: Calculated Energies (hartrees), Energy Difference ΔE Relative to 1*H*-ANTA (kcal/mol), Unscaled Zero-Point Vibrational Energies ZPE (kcal/mol), and Total Dipole Moment (D) for ANTA Tautomers and Radicals

compound	calculation level	energy	ΔE	ZPE	dipole
1*H*-ANTA	HF/6-31G(d,p)	−499.3087356		54.4474	3.34
	HF/6-311+G(d,p)	−499.4375777		54.0747	3.33
	MP2/6-31G(d,p)	−500.7684825		50.2799	3.62
	MP2/6-311G(d,p)	−500.9694659		50.0538	3.58
	MP2/6-311+G(d,p)	−500.9958557		49.5315	3.61
	MP4/6-311+G(d,p)[b]	−501.0870627			3.61
	MP2/6-311+G(2d,2p)[c]	−501.1080610			3.56
	MP4/6-311+G(2d,2p)[c]	−501.2011890			3.56
	B3LYP/6-31G(d,p)	−502.1088303		49.6371	3.79
	B3LYP/6-311+G(d,p)	−502.2549129		49.2867	3.91
	BLYP/6-31G(d,p)	−502.0232602		47.4364	4.00
	BLYP/6-311+G(d,p)	−502.1804768		47.1120	4.23
2*H*-ANTA	HF/6-31G(d,p)	−499.3116256	−1.81	54.3676	8.39
	HF/6-311+G(d,p)	−499.4404314	−1.79	54.0079	8.46
	MP2/6-31G(d,p)	−500.7660934	1.50	50.3050	8.35
	MP2/6-311G(d,p)	−500.9670068	1.54	50.0417	8.37
	MP2/6-311+G(d,p)	−500.9933532	1.57	49.7216	8.45
	MP4/6-311+G(d,p)[b]	−501.0856723	0.87		8.45
	MP2/6-311+G(2d,2p)	−501.1043438	2.33		2.33
	MP4/6-311+G(2d,2p)[c]	−501.1986527	1.59		8.31
	B3LYP/6-31G(d,p)	−502.1069149	1.21	49.6016	8.09
	B3LYP/6-311+G(d,p)	−502.2530265	1.19	49.2584	8.42
	BLYP/6-31G(d,p)	−502.0198876	2.11	47.3694	7.98
	BLYP/6-311+G(d,p)	−502.1770976	2.12	47.0466	8.45
4*H*-ANTA	HF/6-31G(d,p)	−499.3000979	5.42	54.0605	6.81
	HF/6-311+G(d,p)	−499.4283765	5.77	53.6752	6.77
	MP2/6-31G(d,p)	−500.7551256	8.38	49.9269	6.79
	MP2/6-311G(d,p)	−500.9555816	8.71	49.7222	6.77
	MP2/6-311+G(d,p)	−500.9815438	8.98	49.2070	6.86
	MP4/6-311+G(d,p)[b]	−501.0745414	7.86		6.86
	MP2/6-311+G(2d,2p)[c]	−501.0944517	8.54		6.79
	MP4/6-311+G(2d,2p)[c]	−501.1893376	7.43		6.79
	B3LYP/6-31G(d,p)	−502.0984973	6.48	49.2256	7.02
	B3LYP/6-311+G(d,p)	−502.2440464	6.82	48.8497	7.26
	BLYP/6-31G(d,p)	−502.0131692	6.32	47.0012	7.06
	BLYP/6-311+G(d,p)	−502.1698299	6.68	46.6571	7.45
4[a]	UHF/6-311+G(d,p)	−295.2691912		42.9919	4.65
	UMP2/6-311+G(d,p)	−296.2028030		40.9989	4.76
	UMP4/6-311+G(d,p)	−296.2696310			4.76
	UB3LYP/6-311+G(d,p)	−297.0033713		39.6329	4.92
5[a]	UHF/6-311+G(d,p)	−443.7177632		34.0535	6.58
	UMP2/6-311+G(d,p)	−445.0571401			6.82
	UMP4/6-311+G(d,p)	−445.1364580			6.82
	UB3LYP/6-311+G(d,p)	−446.1689237		30.8372	5.95
6[a]	UHF/6-311+G(d,p)	−498.8095435		44.2467	7.39
	UMP2/6-311+G(d,p)	−500.3249078			6.92
	UMP4/6-311+G(d,p)	−500.4170270			6.92
	UB3LYP/6-311+G(d,p)	−501.5947924		40.7957	7.94
NO_2	UHF/6-311+G(d,p)	−204.0927603		6.1697	0.67
	UMP2/6-311+G(d,p)	−204.6716372		6.6281	0.71
	UMP4/6-311+G(d,p)	−204.7022300			0.71
	UB3LYP/6-311+G(d,p)	−205.1406953		5.5141	0.34
NH_2	UHF/6-311+G(d,p)	−55.5819975		12.7610	2.13
	UMP2/6-311+G(d,p)	−55.7393111		12.1989	2.14
	UMP4/6-311+G(d,p)	−55.7590590			2.14
	UB3LYP/6-311+G(d,p)	−55.9003804		11.8687	2.08
H	UHF/6-311+G(d,p)	−0.4998098			
	UMP2/6-311+G(d,p)	−0.4998098			
	UMP4/6-311+G(d,p)	−0.4998098			
	UB3LYP/6-311+G(d,p)	−0.5021559			

[a] Defined in Figure 2. [b] Calculated at the optimized MP2/6-311+G(d,p) configuration. [c] Calculated at the optimized MP2/6-311+G(2d,2p) configuration.

ANTA and 4*H*-ANTA. The major differences between the MP2/6-311+G(d,p) values for the three tautomers are in the twist of the NO_2 group, i.e., for 1*H*- and 4*H*-ANTA the twist is very small compared to those in 2*H*-ANTA. However, in both the 1*H*- and 4*H*-ANTA structures, the NH_2 group is pyramidal.

Energies. The absolute and relative (ΔE) energies, together with zero-point vibrational energies at various levels are given in Table 2 for the three tautomers. In the calculation of the relative energies the energy of 1*H*-ANTA was taken as reference.

At the HF level it appears that 2*H*-ANTA is the most stable tautomer, in agreement with the findings of De Paz and Ciller[7] based on results at the HF/3-21G and HF/6-31G levels. However, the order of stability is reversed when electron correlation contributions are taken into account at the MP2, MP4, and DFT levels. Indeed, at the MP2 level, 2*H*-ANTA is

TABLE 3: Scaled Harmonic Vibrational Frequencies (cm^{-1}) Calculated at the MP2/6-311+G(d,p) Level for 1*H*-, 2*H*-, and 3*H*-ANTA Molecules and the Predicted Frequencies by the Force Field (ν_{calc}), Eq 1[a]

mode	assignment[b]	2*H*-ANTA	1*H*-ANTA	3*H*-ANTA	ν_{calc}	$\nu_{calc} - \nu_{MP2}$
ν_1	NO_2 torsion	51.65	40.51	55.42	48.41	7.9
ν_2	skeletal def	138.24	150.08	139.25	136.37	−13.7
ν_3	NO_2 rock	187.10	192.33	186.17	178.84	−13.4
ν_4	NH_2 rock	267.25	204.63	222.80	218.63	14.0
ν_5	skeletal def	304.98	301.08	291.56	277.77	−23.3
ν_6	ring def	373.81	369.99	360.42	349.44	−20.5
ν_7	C−NO_2 def	406.92	408.37	411.45	402.70	−5.6
ν_8	NO_2 def	414.95	455.41	467.05	454.97	−0.4
ν_9	NH_2 def	538.32	516.66	534.59	506.60	−10.0
ν_{10}	ring torsion+NO_2 def	598.30	619.48	571.60	619.91	0.4
ν_{11}	ring torsion	618.40	634.64	611.71	635.49	0.8
ν_{12}	ring+NO_2+NH_2 def	636.01	701.11	651.54	691.41	6.5
ν_{13}	ring torsion	694.48	705.66	694.05	707.61	−1.9
ν_{14}	ring torsion	730.42	730.15	753.14	739.47	9.3
ν_{15}	NO_2 def+ring def	804.13	808.07	796.58	813.83	5.7
ν_{16}	$N_4-C_5-N_1$ bend	964.41	961.19	971.42	952.76	−8.4
ν_{17}	$N_1-N_2-C_3$ bend	1008.36	1009.59	982.89	1007.07	−2.5
ν_{18}	ring def	1055.34	1078.54	1058.91	1077.78	−0.7
ν_{19}	N−N sym str	1154.71	1156.68	1096.52	1160.24	3.5
ν_{20}	NO_2-sym str	1222.44	1267.54	1131.58	1266.63	−0.9
ν_{21}	ring def+N−H bend	1305.64	1287.63	1297.41	1283.57	−4.0
ν_{22}	C−NO_2 sym str	1328.00	1374.48	1401.48	1369.86	−4.6
ν_{23}	ring def	1452.03	1404.07	1407.70	1406.11	2.0
ν_{24}	C−N sym str	1467.84	1453.28	1462.62	1456.87	3.5
ν_{25}	C−NH_2 asym str+NH_2 bend	1498.92	1531.08	1517.41	1532.50	1.4
ν_{26}	C−NH_2 sym str+NH_2 bend	1574.63	1590.37	1579.85	1596.57	6.2
ν_{27}	N−O asym str	1688.86	1699.00	1687.93	1705.18	6.1
ν_{28}	N−H sym str (NH_2)	3421.87	3404.68	3392.28	3402.34	−2.3
ν_{29}	N−H str (N_1-H_{12})	3475.48	3479.87	3473.86	3478.11	−1.7
ν_{30}	N−H asym str (NH_2)	3531.91	3505.55	3490.57	3504.62	−0.9

[a] The differences of the predicted to the calculated MP2 vibrations for 2*H*-ANTA are also indicated. [b] The assignment is based on the values determined for 2H-ANTA. The legend of abbreviations used in text is: def=deformation; str=strectching; asym=asymmetric; symm=symmetric.

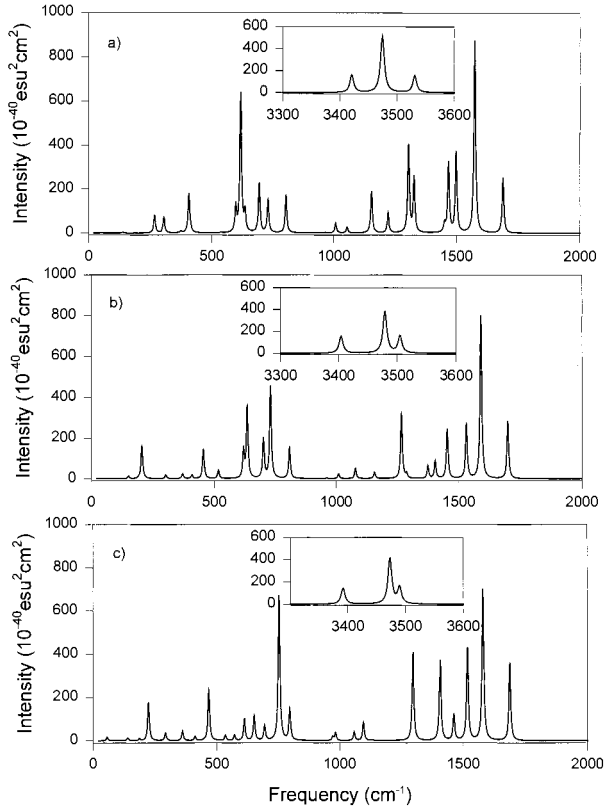

Figure 3. Infrared spectra of the (a) 1*H*-ANTA, (b) 2*H*-ANTA, and (c) 3H-ANTA molecules calculated at the MP2/6-311+G(d,p) level.

less stable than 1*H*-ANTA by about 1.5 kcal/mol, while 4*H*-ANTA is less stable by about 8.9 kcal/mol. To determine the effect of higher order correlations on the relative stabilities, we have determined the MP4 energies (with singles, doubles, triples, and quadruples corrections included) of the optimized MP2 structures. As can be seen from Table 2, the relative energies are slightly decreased going from MP2 to MP4. At the MP4/6-311+G(d,p) level 2*H*-ANTA and 4*H*-ANTA are less stable, respectively, by 0.87 and 7.86 kcal/mol relative to 1*H*-ANTA.

Further insight into the relative energies of these tautomers has been obtained by increasing the basis with an additional set of d and p functions. The corresponding energies at the MP2 and MP4 levels using the basis 6-311+G(2d,2p) are given Table 2. In the case of 2*H*-ANTA the new basis set gives an increase of about 0.7 kcal/mol of the relative energy ΔE at both the MP2 and MP4 levels. However, in the case of 4*H*-ANTA the corresponding relative energy decreases by about 0.4 kcal/mol. Given the small difference in energies for 1*H*- and 2*H*-ANTA, it is expected that both tautomers should be detectable experimentally. However, as already pointed out, in solid polymorphs only the 2*H*-ANTA tautomer has been identified.[5,6] Thus, we investigated (see below) the effects of dipolar interactions on the relative stabilities of the two tautomers in solutions.

The relative stabilities of the various tautomers are also maintained at the DFT level (1*H*-ANTA > 2*H*-ANTA > 4*H*-ANTA), but the absolute differences vary slightly. At the B3LYP level, the predicted energy difference relative to the structure of 1*H*-ANTA is about 1.2 kcal/mol for 2*H*-ANTA and between 6.5 and 6.8 kcal/mol for 4*H*-ANTA, depending on the basis set. These results are closer to the corresponding MP2 predictions than are the BLYP values. At the BLYP level, the energy difference between 2*H*-ANTA and 1*H*-ANTA is 2.1 kcal/mol, while 4*H*-ANTA is predicted to have an energy between 6.3 and 6.7 kcal/mol higher than 1*H*-ANTA.

TABLE 4: Bond Dissociation Energies (in kcal/mol) for 2*H*-ANTA

process	UHF/6-311+G(d,p)	UMP2/6-311+G(d,p)	UMP4/6-311+G(d,p)	UB3LYP/6-311+G(d,p)
2*H*-ANTA → **4** + NO_2	44.9	70.3	67.1	64.1
2*H*-ANTA → **5** + NH_2	81.8	117.3	112.8	108.8
2*H*-ANTA → **6** + H	73.5	97.1	97.2	89.0

TABLE 5: Calculated Energies (au), Zero-Point Vibrational Energies ZPE (kcal/mol), and Dipole Moments (D) and the Energy Differences $\Delta E = E_{2H-ANTA} - E_{1H-ANTA}$ (kcal/mol) for 1*H*-ANTA and 2*H*-ANTA Molecules at the B3LYP/6-311++G(d,p) Level for Various Values of the Dielectric Constant ϵ

ϵ		1*H*-ANTA	2*H*-ANTA	ΔE
1.0	energy	−502.2606567	−502.2587476	−1.19
	dipole moment	3.91	8.42	
4.806	energy	−502.2630230	−502.2695912	4.12
	ZPE	49.12	49.02	
	dipole moment	4.87	10.56	
18.5	energy	−502.2639290	−502.2737697	6.17
	ZPE	49.06	48.83	
	dipole moment	5.26	11.42	
78.4	energy	−502.2642242	−502.2751355	6.84
	ZPE	49.03	48.68	
	dipole moment	5.39	11.73	

TABLE 6: Influence of Dielectric Constant ϵ on the Equilibrium Geometries of 1*H*- and 2*H*-ANTA[a]

parameter	$\epsilon = 1$	$\epsilon = 4.806$	$\epsilon = 18.5$	$\epsilon = 78.4$
		1*H*-ANTA		
$r(C_3-N_9)$	1.3679	1.3625 (0.4)	1.3603 (0.6)	1.3594 (0.6)
$r(C_5-N_6)$	1.4524	1.4462 (0.4)	1.4442 (0.6)	1.4432 (0.6)
$\theta(C_3-N_9-H_{10})$	116.18	116.85 (0.6)	117.12 (0.8)	117.28 (0.9)
$\theta(C_3-N_9-H_{11})$	115.51	116.50 (0.9)	116.87 (1.2)	117.06 (1.3)
$\theta(H_{10}-N_9-H_{11})$	115.50	116.00 (0.4)	116.20 (0.6)	116.35 (0.7)
$\theta(C_5-N_6-O_7)$	115.56	115.72 (0.3)	115.87 (0.4)	115.91 (0.5)
$\theta(C_5-N_6-O_8)$	118.18	118.36 (0.2)	118.43 (0.2)	118.46 (0.2)
$\theta(O_7-N_6-O_8)$	126.46	125.92 (0.4)	125.70 (0.6)	125.63 (0.7)
$\tau(N_2-C_3-N_9-H_{10})$	20.56	17.81	16.75	16.32
$\tau(N_4-C_3-N_9-H_{11})$	−22.19	−21.69	−21.45	−20.90
$\tau(N_1-C_5-N_6-O_7)$	0.29	0.17	0.13	0.07
$\tau(N_4-C_5-N_6-O_8)$	0.04	0.29	0.39	0.43
		2*H*-ANTA		
$r(C_3-N_9)$	1.3693	1.3524 (1.2)	1.3457 (1.7)	1.3432 (1.9)
$r(C_5-N_6)$	1.4689	1.4626 (0.4)	1.4599 (0.6)	1.4588 (0.7)
$\theta(C_3-N_9-H_{10})$	117.49	120.78 (2.8)	122.15 (4.0)	122.74 (4.5)
$\theta(C_3-N_9-H_{11})$	113.46	116.94 (3.1)	118.37 (4.3)	118.94 (4.8)
$\theta(H_{10}-N_9-H_{11})$	113.78	116.41 (2.3)	117.47 (3.2)	117.94 (3.7)
$\theta(C_5-N_6-O_7)$	117.14	117.76 (0.5)	118.03 (0.8)	118.13 (0.8)
$\theta(C_5-N_6-O_8)$	116.63	117.16 (0.4)	117.36 (0.6)	117.43 (0.7)
$\theta(O_7-N_6-O_8)$	126.23	125.08 (0.9)	124.61 (1.3)	124.44 (1.4)
$\tau(N_2-C_3-N_9-H_{10})$	35.81	19.27	10.88	−4.73
$\tau(N_4-C_3-N_9-H_{11})$	−11.68	−11.68	−7.55	3.35
$\tau(N_1-C_5-N_6-O_7)$	−2.29	−0.57	−0.18	−0.02
$\tau(N_4-C_5-N_6-O_8)$	−2.63	−0.57	−0.14	−0.03

[a] Only those coordinates that are most strongly affected by the media are given. The values in parentheses are the absolute percentage differences compared to the $\epsilon = 1$ geometry.

Vibrational Frequencies. The ab initio calculated fundamental vibrational frequencies of the ANTA tautomers are given in Table 3 and supplemental Tables 4S and 5S for several levels of theory. These frequencies have been scaled by empirical factors, as discussed in section 2, to correct for the over estimation of the vibrational frequencies at these levels of theory. Since there are no experimental or theoretical values for the fundamental frequencies available for either gas or solid phases of ANTA, we will consider the scaled frequencies determined at the MP2/6-311+G(d,p) level as the reference. The simulated IR spectra calculated at the MP2/6-311+G(d,p) level for all three tautomers are shown in Figure 3.

Approximate descriptions of the fundamental modes for 2*H*-ANTA are given in Table 3. This assignment is based on visual inspection of the MP2/6-311+G(d,p) eigenvectors. By comparison the dependence of the calculated frequencies on the basis set used in MP2 calculations (see Tables 4s and 5S), it is observed that the agreement of these sets of values with the MP2/6-311+G(d,p) results is generally good. The overall root-mean-square (rms) deviations are 2.17 and 1.95 cm^{-1} at the MP2/6-31G(d,p) and MP2/6-311G(d,p) levels, respectively, with the largest deviations of 44 and 29 cm^{-1} for the mode ν_8.

The vibrational frequencies calculated using DFT are given in Table 4 S. Generally, there is good agreement between the scaled B3LYP and BLYP frequencies and the corresponding MP2/6-311+G(d,p) values, with rms deviations of 5.05 cm^{-1} at B3LYP/6-31G(d,p), 5.94 cm^{-1} at B3LYP/6-311+G(d,p), 5.59 cm^{-1} at BLYP/6-31G(d,p), and 6.81 cm^{-1} at BLYP/6-311+G(d,p) levels.

For the 1*H*-ANTA and 4*H*-ANTA the variations of the frequencies with the basis set and level of calculation remain in the same range of values. For example, the rms values at the MP2 level of 1*H*-ANTA are, respectively, 3.10% and 3.39% at the MP2/6-31G(d,p) and MP2/6-311G(d,p), and 2.02% and 3.03% at the same levels for 4*H*-ANTA. On the other hand, the rms variations at the B3LYP/6-311+G(d,p) and BLYP/6-311+G(d,p) levels are, respectively, 6.78% and 7.38% for 1*H*-ANTA and 5.60% and 7.10% for 4*H*-ANTA.

Bond Dissociation Energies. Identification of the initial mechanistic steps in thermal reactions of energetic materials is important. The reactions are often very complex. For example, in the case of the thermal decomposition of crystalline NTO, several mechanistic steps, such as the autocatalytic mechanism,[31] nitrogen−hydrogen bond cleavage,[32] NO_2 elimination with formation of amide fragments,[33,34] or hydrogen transfer to the nitro groups, followed by subsequent loss of HONO, have been proposed.[35] In the case of ANTA, kinetic data related to the initial reaction steps are not available at present, but it is expected that processes of the type postulated for NTO are involved.

An estimate of the energy required to produce homolytic bond cleavages can be obtained by calculating the corresponding bond dissociation energies. We have done such calculations for the 2*H*-ANTA tautomer for the particular case of $C-NO_2$, $C-NH_2$, and N_2-H_{12} bonds. For this purpose we have used the energies of the optimized structures and radicals obtained at (U)HF, (U)MP2, (U)MP4, and B3LYP levels and corrected for zero-point vibrational energy (ZPE). For consistency in all cases, ZPEs were obtained from the UHF/6-311+G(d,p) frequencies scaled by 0.897. The energies of the radicals **4**, **5**, and **6** (shown in Figure 2) involved in these bond cleavages are given in Table 2 together with the corresponding energies for NO_2, NH_2, and H. The final results for the bond dissociation energies are given in Table 4.

The bond dissociation energies calculated at the UMP4/6-311+G(d,p) level are between the values predicted at B3LYP/6-311+G(d,p) and UMP2/6-311+G(d,p) levels (see Table 4). In the case of the $C-NO_2$ bond, the spread of the B3LYP and UMP2 values relative to the UMP4 results is about 3 kcal/mol, while in the case of $C-NH_2$ the bond strength values differ by 3.9 and 4.4 kcal/mol, respectively. Much better agreement between the UMP4 and UMP2 results is obtained in the case

TABLE 7: The Force Field Parameters for Gas-Phase 2*H*-ANTA

bond	r^0 (Å)	k_r (kcal/mol Å^{-2})	bond angle	θ^0 (deg)	k_θ (kcal/mol rad^{-2})
N_1-N_2	1.35418	625.42	$N_1-N_2-C_3$	111.07	464.97
N_2-C_3	1.35956	247.14	$N_2-N_1-C_5$	99.99	345.71
C_3-N_4	1.32852	439.28	$C_3-N_4-C_5$	101.40	206.41
N_4-C_5	1.35181	686.08	$N_1-C_5-N_4$	117.75	208.40
C_5-N_1	1.33064	557.40	$N_1-C_5-N_6$	120.50	225.57
C_5-N_6	1.45730	593.36	$N_4-C_5-N_6$	121.75	321.45
N_6-O_7	1.23100	486.40	$C_5-N_6-O_8$	116.93	293.39
N_6-O_8	1.23100	565.17	$C_5-N_6-O_7$	116.51	350.06
C_3-N_9	1.38250	606.92	$O_8-N_6-O_7$	126.56	287.40
N_9-H_{10}	1.01230	934.30	$N_2-C_3-N_9$	123.58	222.45
N_9-H_{11}	1.01270	963.80	$N_4-C_3-N_9$	126.63	485.73
N_2-H_{12}	1.01120	958.80	$C_3-N_9-H_{10}$	114.34	68.20
			$C_3-N_9-H_{11}$	110.84	47.12
			$H_{10}-N_9-H_{11}$	111.20	42.21
			$N_1-N_2-H_{12}$	119.59	99.17
			$C_3-N_2-H_{12}$	129.34	27.78

wag angle	γ^0 (deg)	k_γ (kcal/mol rad^{-2})
$N_1-C_5-N_4-N_6$	0.00	44.50
$N_2-C_3-N_4-N_9$	0.00	19.62
$C_3-N_2-N_1-H_{12}$	0.00	73.69

dihedral angle	τ^0 (deg)	a_0 (kcal/mol)	a_2 (kcal/mol)	a_4 (kcal/mol)
$O_8-N_6-C_5-N_4$	−22.47	6.265	−8.860	3.130
$O_7-N_6-C_5-N_1$	−22.25	6.418	−9.076	3.181
$H_{11}-N_9-C_3-N_4$	−2.61	17.977	−24.003	6.026
$H_{10}-N_9-C_3-N_2$	50.74	5.268	3.886	4.881
$N_4-C_3-N_2-N_1$	0.00	2.110	−2.110	0.000
$C_3-N_2-N_1-C_5$	0.00	1.800	−1.800	0.000
$N_9-C_3-N_2-H_{12}$	0.00	2.200	−2.200	0.000
$N_4-C_3-N_2-H_{12}$	180.00	1.800	−1.800	0.000
$N_6-C_5-N_1-N_2$	180.00	1.760	−1.760	0.000

of N_2-H_{12} bond energy where the predicted values are practically identical.

The UMP4 bond dissociation energies suggest that $C-NO_2$ bond cleavage might play an important role in thermal reactions of ANTA. The value of 67.1 kcal/mol obtained in this study lies between the experimental value of 62 kcal/mol for nitroethane[36] and 71.4 ± 2.0 kcal/mol determined for nitrobenzene.[37] In addition, our calculated bond energy is in excellent agreement with the value of 67 kcal/mol recently reported by Meredith et al.[38] for the $C-NO_2$ bond in NTO. Similarly, the calculated dissociation energy of 97.2 kcal/mol for the N_2-N_{12} bond is slightly higher than the value of 94.6 kcal/mol determined at the UMP2 level by Harris and Lammertsma[39] for the N−H bond in NTO.

As mentioned above, hydrogen atom transfer has been proposed to be one of the reaction channels in NTO condensed phase reactions. On the basis of the close proximity of the N−H bond dissociation energies in ANTA and NTO and the similarity of these two molecules, it seems likely that hydrogen atom transfer may be involved in thermal reactions of ANTA in the solid phase.

Finally, the large value of 112.8 kcal/mol for the bond dissociation energy of the $C-NH_2$ bond in ANTA suggests that thermal elimination of the amino group is not a favored channel.

Solvation Effects. The results of the previous sections have indicated that at the MP2, MP4, and DFT levels 1*H*-ANTA is slightly more stable in the gas phase than the 2*H*-ANTA tautomer. However, by inspecting the calculated dipole moments of these tautomers (given in Table 2) we observe that 2*H*-ANTA has a dipole moment greater than 1*H*-ANTA. For example, at the MP2/6-311+G(d,p) level, the values of the dipole moments for 2*H*-ANTA and 1*H*-ANTA are 8.45 and 3.61 D, respectively. The large difference in the sizes of the dipole moments of these tautomers is expected to determine their relative stability in a polar solvent.

To investigate the effects of solvation on the structure and energetics of ANTA, we have optimized the structures of 1*H*-ANTA and 2*H*-ANTA tautomers within the Onsager reaction field model. We have considered four values of the dielectric constant for the solute: $\epsilon = 1.0$ (corresponding to the gas phase), $\epsilon = 4.806$ (corresponding to chloroform), $\epsilon = 18.5$ (corresponding to 2-butanone), and $\epsilon = 78.4$ (corresponding to water). Geometry optimizations were carried out at the B3LYP/6-311++G(d,p) level. The total energies are given in Table 5.

From the analysis of the results in Table 5, we observe that 1*H*-ANTA is the most stable for $\epsilon = 1.0$ while in solvents of different polarity, i.e., $\epsilon \geq 4.8$, the 2*H*-ANTA tautomer is the most stable. This is in agreement with experimental findings, which indicate that 2*H*-ANTA is the most stable tautomer in a polar solvent.[5,6] Moreover, it is seen that increasing the solvent dielectric constant results in an increase in the energy difference between the 2*H*- and 1*H*-ANTA tautomers. Indeed, the calculated energy difference varies from 4.12 kcal/mol at $\epsilon = 4.806$ to 6.84 kcal/mol at $\epsilon = 78.4$.

The effects of varying the dielectric constant on the structures of 1*H*- and 2*H*-ANTA are illustrated by the results in Table 6, where we give only those parameters having the largest variations as functions of ϵ. As expected, due to a larger interaction with the solvent, the 2*H*-ANTA molecule displays the largest modifications of the internal parameters with changing ϵ. The results in Table 6 show that the geometrical parameters most influenced by the media are those describing the orientations of the amino and nitro groups relative to the molecular ring. There are significant variations in the dihedral angles. For example, the dihedral angles $\tau(N_2-C_3-N_9-H_{10})$ and $\tau(N_4-C_3-N_9-H_{11})$ in 2*H*-ANTA vary, respectively, from

35.81° to −11.68° for $\epsilon = 1.0$, and −4.73° to 3.35° for $\epsilon = 78.4$. The degree of pyramidalization of the NH_2 group decreases with increasing dielectric constant. The NO_2 plane becomes practically coincident with the plane of the ring for $\epsilon = 78.4$. These modifications of the molecular configuration agree well with the experimental findings for β-ANTA[6] (also see Table 1). Similarly, the length of the C−NO_2 bond varies from 1.468 to 1.458 Å and the C−NH_2 bond from 1.369 to 1.342 Å. This is in accordance with the effects found experimentally for the β-ANTA[6] structure, where these bond lengths are 1.445 and 1.333 Å, respectively.

These results indicate energetic and geometric changes due to solvation similar to those observed in the solid phase. Although full ab initio calculations for the crystal phase are needed for an accurate description, the reaction field theory calculations provide qualitative insight into the solvent effects on equilibrium structures and energies of the two tautomers.

Equilibrium Force Fields. The values of the geometric and spectroscopic results calculated for gas-phase 2*H*-ANTA were used to construct an equilibrium force field. The intramolecular motions are described by a classical potential constructed as superpositions of harmonic bond stretches, bond and wag angles, and a truncated cosine series for the torsional angles of the form

$$V = \sum_{i=1}^{12} \frac{k_{b,i}}{2}(r - r_i^0)^2 + \sum_{i=1}^{16} \frac{k_{\theta,i}}{2}(\theta - \theta_i^0)^2 + \sum_{i=1}^{3} \frac{k_{\gamma,i}}{2}(\gamma - \gamma_i^0)^2 + \sum_{i=1}^{9}[\sum_{j=0}^{2} a_{2j} \cos(2j\tau)]_i \quad (1)$$

The parameters r^0, θ^0, γ^0, and a_{2j} in eq 1 were adjusted to reproduce the MP2/6-311+G(d,p) equilibrium geometry given in Tables 1 and 1S. The force constants k_b, k_θ, k_γ, and a_{2j} were adjusted to yield reasonable agreement with the scaled ab initio MP2/6-311+G(d,p) frequencies. A complete list of the parameters used in eq 1 is given in Table 7.

A normal-mode analysis at the equilibrium geometry predicted by eq 1 provides a check of the accuracy of the calculated force field. The computed vibrational frequencies are given in Table 3. There is good agreement between the scaled ab initio values and the vibrational frequencies predicted by our proposed force field, as shown by the small differences given in parentheses in Table 3. The overall rms deviation between the two sets of values is 8.51 cm^{-1}, with the largest difference being 23.3 cm^{-1} for the low-frequency mode ν_5.

4. Concluding Remarks

Ab initio molecular orbital calculations were performed to predict the structures, fundamental vibrational frequencies, and the relative stability of the ANTA tautomers.

The 1*H*-ANTA tautomer is the most stable at the HF level while MP2, MP4, and DFT predict 2*H*-ANTA to be most stable. The results suggest that both these tautomers could be observed in the gas phase.

There is relatively good agreement between the geometries of the 2*H*-ANTA molecule in the gas and solid phases, except for the twist angles of the NO_2 group, which are much larger in the gas phase than in the crystalline α phase.

The results of DFT calculations using B3LYP and BLYP functionals indicate that these are good alternatives to the more demanding MP2 calculations when the geometrical structures, harmonic vibrations, and the relative stability of various tautomers are of interest. The largest deviations of the B3LYP and BLYP geometrical parameters from the corresponding MP2 values are about 1.8% for bond lengths and 2.7% for bond angles. Similarly, the fundamental frequencies, as calculated with these two functionals, are generally close to those determined at the MP2 level.

The results of geometry optimizations when solvent effects were considered indicate that 2*H*-ANTA becomes the most stable tautomer, in agreement with experimental findings. Moreover, the increase of the dielectric constant of the solvent from 4.8 to 18.5 to 78.4 D yields a better agreement of the calculated geometrical parameters of 2*H*-ANTA with the experimental condensed phase structure, particularly the β-ANTA structure.

The predicted ab initio results for the geometry and vibrational frequencies obtained at the MP2/6-311+G(d,p) level for 2*H*-ANTA were used to construct a valence force field. The results of a normal-mode analysis show that the semiempirical potential accurately reproduces the ab initio results.

The results of this study provide a better understanding of the structural, spectroscopic, and energetic differences among the ANTA tautomers in the gas phase as well as estimates of the effects of solvation on these parameters.

Acknowledgment. This work was supported by the Air Force Office of Scientific Research under Grants F49620-93-l-0237 and F49620-95-l-0411. We gratefully acknowledge a supercomputer allocation at ASC MSRC (Wright-Patterson Air Force Base). We are grateful to Dr. Cary Chabalowski, Army Research Laboratory, Aberdeen, MD, for providing the program for representing the ab initio spectra.

Supporting Information Available: Tables 1S−5S giving geometrical parameters and vibrational frequencies for 1*H*-, 2*H*-, and 3*H*-ANTA (10 pages). Ordering information is given on any current masthead page.

References and Notes

(1) Lee, K.-Y.; Storm, C. B.; Hiskey, M. A.; Coburn, M. D. *J. Energ. Mater*. **1991**, *9* 415.
(2) Lee, K.-Y.; Coburn, M. D.; Hiskey, M. A. Los Alamos National Laboratory Report, LA-12582-MS, June 1993.
(3) Dick, J. J.; Ritchie, J. P. *J. Appl. Phys*. **1994**, *76*, 2726.
(4) Botcher, T. R.; Beardall, D. J.; Wight, C. A.; Fan, L.; Burkey, T. J. *J. Phys. Chem.* **1996**, *100*, 8802.
(5) Garcia, E.; Lee, K.-Y. *Acta Crystallogr*. **1992**, *C48*, 1682.
(6) Lee, K.-Y.; Gilardi, R.; Hiskey, M. A.; Stine, J. R. *Mater. Res. Soc. Symp. Proc.* **1996**, *418*, 43.
(7) De Paz, J.-L. G.; Ciller, J. *Propellants, Explos., Pyrotech.* **1994**, *19* 32.
(8) Hehre, W.; Radom, L.; Schleyer, P. v. R.; Pople, J. A. *Ab Initio Molecular Orbital Theory*; Wiley-Interscience: New York, 1986.
(9) (a) Moller, C. M. S. *Phys. Rev*. **1934**, *46*, 618. (b) Hehre, W. J.; Ditchfield, R.; Pople, J. A. *J. Chem. Phys*. **1972**, *56*, 2257. (c) Hariharan, P. C.; Pople, J. A. *Theor. Chim. Acta* **1973**, *28*, 213. (d) Gordon, M. S. *Chem. Phys. Lett*. **1980**, *76*, 163.
(10) (a) Hohenber, P.; Kohn, W. *Phys. Rev. B*: *Condens. Matter* **1964**, *126*, 864. (b) Parr, R. G.; Yand, W. *Density-Functional Theory of Atoms and Molecules*; Oxford University Press: New York, 1989.
(11) Rauhut, G.; Pulay, P. *J. Phys. Chem*. **1995**, *99*, 3093.
(12) Deng, L.; Ziegler, T. *J. Phys. Chem*. **1995**, *99*, 612.
(13) Pai, S. V.; Chabalowski, C. F.; Rice, B. M. *J. Phys. Chem*., **1996**, *100*, 15368.
(14) Scott, A. P.; Radom, L. *J. Phys. Chem*. **1996**, *100*, 16502.
(15) Sorescu, D. C.; Sutton, T. R. L.; Thompson, D. L.; Beardall, D.; Wight, C. A. *J. Mol. Struct*. **1996**, *384*, 87.
(16) Becke, A. D. *J. Chem. Phys*. **1993**, *98*, 5648.
(17) Lee, C.; Yang, W.; Parr, R. G. *Phys. Rev. B: Condens. Matter* **1988**, *41*, 785.
(18) Forseman, J. B.; Frisch, A. In *Exploring Chemistry with Electronic Structure Methods*; Gaussian, Inc.: Pittsburgh, PA, 1996.
(19) Sewell, T. D.; Thompson, D. L. *J. Phys. Chem*. **1991**, *95*, 6228.
(20) Shalashilin, D. V.; Thompson, D. L. *J. Phys. Chem*. **1997**, *101*, 961.

(21) Sorescu, D. C.; Thompson, D. L.; Raff, L. M. *J. Chem. Phys*. **1995**, *102*, 7910.
(22) Sorescu, D. C.; Thompson, D. L.; Raff, L. M. *J. Chem. Phys*. **1995**, *103*, 5387.
(23) Frisch, M. J.; Trucks, G. W.; Schlegel, H. B.; Gill, P. M. W.; Johnson, B. G.; Wong, M. W.; Foresman, J. B.; Robb, Cheeseman, J. R.; Keith, T.; Petersson, G. A.; Montomery, J. A.; Raghavachari, K.; Al-Laham, M. A.; Zakrzewski, V. G.; Ortiz, J. V.; Foresman, J. B.; Cioslowski, J.; Stefanov, B. B.; Nanayakkara, A.; Challacombe, M.; Peng, C. Y.; Ayala, P. Y.; Chen, W.; Wong, M. W.; Andres, J. L.; Replogle, E. S.; Gomperts, R.; Martin, R. L.; Fox, D. J.; Binkley, J. S.; Defrees, D. J.; Baker, J.; Stewart, J. J. P.; Head-Gordon, J.; Gonzalez, C.; Pople, J. A. *Gaussian-94, Revision E.2*; Gaussian, Inc.: Pittsburgh, PA, 1995.
(24) Clark, T.; Chandrasekar, J.; Spitznagel, G. W.; Shleyer, P. v. R. *J. Comput. Chem*. **1983**, *4*, 294.
(25) Becke, A. D. *Phys. Rev. A: At., Mol., Opt. Phys.* **1988**, *38*, 3098.
(26) Riggs, N. V.; Zoller, U.; Nguyen, M. T.; Radom, L. *J. Am. Chem. Soc*. **1992**, *114*, 4354.
(27) Onsager, L. *J. Am. Chem. Soc*. **1938**, *58*, 1486.
(28) Wong, M. W.; Frisch, M. J.; Wiberg, K. B. *J. Am. Chem. Soc*. **1991**, *113*, 4776.
(29) Payne, P. W.; Allen, L. C. In *Applications of Electron Structure Theory*; Schaefer, H. F., III, Ed.; Plenum Press: New York, 1977.
(30) Williams, D. E. In *Crystal Cohesion and Conformational Energies*; Metzger, R. M., Ed.; Springer-Verlag: Berlin, 1981.
(31) Rothgery, E. F.; Audetter, D. E.; Wedlich, R. C.; Csejka, D. A. *Thermochim. Acta* **1991**, *185*, 235.
(32) Menapace, J. A.; Marlin, J. E.; Bruss, D. R.; Dascher, R. V. *J. Phys. Chem*. **1991**, *95*, 5509.
(33) Östmark, H.; Bergman, H.; Åqvist, G.; Langlet, A.; Persson, B. *Proc. Int. Pyrotech. Semin.* **1991**, *16*, 874.
(34) Prabhakaran, K. V.; Naidu, S. R.; Kurian, E. M. *Thermochim. Acta* **1994**, *241*, 199.
(35) Oxley, J. C.; Smith, J. L.; Zhou, Z. *J. Phys. Chem.* **1995**, *99*, 10383.
(36) *CRC Handbook in Chemistry and Physics*, 65th ed.; Weast, R. C., Ed.; CRC Press, Inc.: Boca Raton, FL, 1983−1985; p F-184.
(37) Gonzales, A. C.; Larson, C. W.; McMillen, D. F.; Golden, D. M. *J. Phys. Chem*. **1985**, *89*, 4809.
(38) Meredith, C.; Russell, T. P.; Mowrey, R. C.; McDonald, J. R. *J. Phys. Chem*., **1998**, *102*, 471.
(39) Harris, N. J.; Lammertsma, K. *J. Am. Chem. Soc*. **1996**, *118*, 8048.